Langmuir
Article
pubs.acs.org/Langmuir

Hydrogen Bonding Effects in Adsorption of Water−Alcohol Mixtures in Zeolites and the Consequences for the Characteristics of the Maxwell−Stefan Diffusivities

Rajamani Krishna* and Jasper M. van Baten

Van't Hoff Institute for Molecular Sciences, University of Amsterdam, Science Park 904, 1098 XH Amsterdam, The Netherlands

Received February 19, 2010. Revised Manuscript Received March 31, 2010

This work highlights a variety of peculiar characteristics of adsorption and diffusion of polar molecules such as water, methanol and ethanol in zeolites. These peculiarities are investigated with the aid of configurational-bias Monte Carlo (CBMC) simulations of adsorption isotherms, and molecular dynamics (MD) simulations of diffusivities in FAU, MFI, DDR, and LTA zeolites.

Because of strong hydrogen bonding, significant clustering of the guest molecules occurs in all investigated structures. Because of molecular clustering, the inverse thermodynamic factor $1/\Gamma_i \equiv (\mathrm{d}[\ln c_i])/(\mathrm{d}[\ln f_i])$ exceeds unity for a range molar concentrations c_i within the micropores. The degree of clustering is lowered as the temperature is increased. For the concentration ranges for which $1/\Gamma_i > 1$, the Fick diffusivity, D_i, for unary diffusion is often lower than both the Maxwell−Stefan, $Đ_i$, and the self-diffusivity, $D_{i,\mathrm{self}}$. For water−alcohol mixtures, the hydrogen bonding between water and alcohol molecules is much more predominant than for water−water, and alcohol−alcohol molecule pairs. Consequently, the adsorption of water−alcohol mixtures shows significant deviations from the predictions of the ideal adsorbed solution theory (IAST). The water−alcohol bonding also leaves its imprint on the mixture diffusion characteristics. The Maxwell−Stefan diffusivity, $Đ_i$, of either component in water−alcohol mixtures is lower than the corresponding values of the pure components; this behavior is distinctly different from that for mixtures of nonpolar guest molecules. The binary exchange coefficient $Đ_{12}$ for water−alcohol mixtures is also significantly lower than either self-exchange coefficients $Đ_{11}$ and $Đ_{22}$ of the constituent species. This implies that correlation effects are significantly stronger in water−alcohol mixtures than for the constituent species. Correlation effects are found to be significant for water−alcohol mixture diffusion in DDR and LTA zeolites, even though such effects are negligible for the pure constituents. The major conclusion to emerge from this investigation is that, unlike mixtures of nonpolar molecules, it is not possible to estimate water−alcohol mixture adsorption and diffusion characteristics on the basis of pure component data.

1. Introduction

Zeolites such as MFI, LTA, DDR, FAU are used as membrane devices in dehydration and pervaporation applications.[1−9] The development of these separation technologies requires a proper understanding and characterization of the adsorption and diffusion of polar molecules such as water, and alcohols inside micropores. For modeling binary mixture permeation, the fluxes N_i are commonly related to the chemical potential gradients $\nabla\mu_i$ by use of the Maxwell−Stefan (M−S) equations[10−20]

$$-\phi\frac{c_i}{RT}\nabla\mu_i = \sum_{\substack{j=1\\ j\neq i}}^{2}\frac{x_jN_i - x_iN_j}{Đ_{ij}} + \frac{N_i}{Đ_i};\quad i = 1,2 \qquad (1)$$

The concentrations c_i are expressed as the number of moles per cubic meter of *accessible* pore volume, and ϕ represents the fractional pore volume. The fluxes N_i are defined in terms of the cross-sectional area of the crystalline framework. The x_i in eq 1 are the component mole fractions of the adsorbed phase within the microporous structures

$$x_i = c_i/c_t;\quad i = 1,2 \qquad (2)$$

The $Đ_i$ characterize species i−wall interactions in the broadest sense. The $Đ_{12}$ are exchange coefficients representing interaction between components i with component j. At the molecular level, the $Đ_{ij}$'s reflect how the facility for transport of species i *correlates*

*Corresponding author. Telephone: +31 20 6270990. Fax: + 31 20 5255604. E-mail: r.krishna@uva.nl..

(1) Caro, J.; Noack, M. *Microporous Mesoporous Mater.* **2008**, *115*, 215–233.
(2) Wee, S. L.; Tye, C. T.; Bhatia, S. *Sep. Purif. Technol.* **2008**, *63*, 500–516.
(3) Bowen, T. C.; Noble, R. D.; Falconer, J. L. *J. Membr. Sci.* **2004**, *245*, 1–33.
(4) Pera-Titus, M.; Fité, C.; Sebastián, V.; Lorente, E.; Llorens, J.; Cunill, F. *Ind. Eng. Chem. Res.* **2008**, *47*, 3213–3224.
(5) Pera-Titus, M.; Llorens, J.; Tejero, J.; Cunill, F. *Catal. Today* **2006**, *118*, 73–84.
(6) Kuhn, J.; Yajima, K.; Tomita, T.; Gross, J.; Kapteijn, F. *J. Membr. Sci.* **2008**, *321*, 344–349.
(7) Kuhn, J.; Castillo-Sanchez, J. M.; Gascon, J.; Calero, S.; Dubbeldam, D.; Vlugt, T. J. H.; Kapteijn, F.; Gross, J. *J. Phys. Chem. C* **2009**, *113*, 14290–14301.
(8) Zhu, G.; Li, Y.; Zhou, H.; Liu, J.; Yang, W. *J. Membr. Sci.* **2009**, *337*, 47–54.
(9) Tokay, B.; Falconer, J. L.; Noble, R. D. *J. Membr. Sci.* **2009**, *334*, 23–39.
(10) Kapteijn, F.; Moulijn, J. A.; Krishna, R. *Chem. Eng. Sci.* **2000**, *55*, 2923–2930.
(11) Skoulidas, A. I.; Sholl, D. S.; Krishna, R. *Langmuir* **2003**, *19*, 7977–7988.
(12) Chempath, S.; Krishna, R.; Snurr, R. Q. *J. Phys. Chem. B* **2004**, *108*, 13481–13491.
(13) Krishna, R.; van Baten, J. M. *J. Phys. Chem. B* **2005**, *109*, 6386–6396.
(14) Krishna, R.; van Baten, J. M. *Ind. Eng. Chem. Res.* **2006**, *45*, 2084–2093.
(15) Krishna, R.; van Baten, J. M. *Microporous Mesoporous Mater.* **2008**, *109*, 91–108.
(16) Krishna, R.; van Baten, J. M. *Chem. Eng. Sci.* **2008**, *63*, 3120–3140.
(17) Krishna, R.; van Baten, J. M. *Chem. Eng. Sci.* **2009**, *64*, 3159–3178.
(18) Krishna, R. *J. Phys. Chem. C* **2009**, *113*, 19756–19781.
(19) van den Bergh, J.; Ban, S.; Vlugt, T. J. H.; Kapteijn, F. *J. Phys. Chem. C* **2009**, *113*, 17840–17850.
(20) Li, S.; Martinek, J. G.; Falconer, J. L.; Noble, R. D.; Gardner, T. Q. *Ind. Eng. Chem. Res.* **2005**, *44*, 3220–3228.

with that of species j. Conformity with the Onsager reciprocal relations prescribes

$$Đ_{12} = Đ_{21} \tag{3}$$

In earlier published work,[15,16] the M−S equations were set up differently using loadings expressed as moles per kilogram of framework. A detailed comparison of the earlier approach with the current one is provided by Krishna and Van Baten;[17] see the Supporting Information accompanying their paper.

The M−S eqs 1 can be rewritten to evaluate the fluxes N_i explicitly for an n-component mixture

$$N_i = -\phi \sum_{j=1}^{n} \Delta_{ij} \frac{c_j}{RT} \nabla \mu_j; \quad i = 1, 2, ..., n \tag{4}$$

The elements Δ_{ij} of the matrix [Δ] are directly accessible from MD simulations[11,12,16,17,21−23]

$$\Delta_{ij} = \frac{1}{2} \lim_{\Delta t \to \infty} \frac{1}{n_j} \frac{1}{\Delta t} \langle (\sum_{l=1}^{n_i} (\mathbf{r}_{l,i}(t+\Delta t) - \mathbf{r}_{l,i}(t))) \bullet (\sum_{k=1}^{n_j} (\mathbf{r}_{k,j}(t+\Delta t) - \mathbf{r}_{k,j}(t))) \rangle \tag{5}$$

Comparing eq 4 with eq 1, we derive the following expression for a binary mixture

$$[\Delta] = \begin{bmatrix} \frac{1}{Đ_1} + \frac{x_2}{Đ_{12}} & -\frac{x_1}{Đ_{12}} \\ -\frac{x_2}{Đ_{12}} & \frac{1}{Đ_2} + \frac{x_1}{Đ_{12}} \end{bmatrix}^{-1} \tag{6}$$

Inversion of the matrix [Δ] yields the values of the M−S coefficients $Đ_1$, $Đ_2$, and $Đ_{12}$.Formally speaking, the M−S eqs 1 serve only to *define* the phenomenological coefficients $Đ_i$ and $Đ_{ij}$. In practice, the application of eq 1 for estimation of the permeation fluxes N_i is based on two tenets. The first tenet is that the $Đ_i$ can be identified with the corresponding M−S diffusivity for *unary* diffusion, evaluated at the same total loading or occupancy θ_t

$$\theta_t = \sum_{i=1}^{n} \theta_i = \sum_{i=1}^{n} \frac{c_i}{c_{i,\text{sat}}} \tag{7}$$

where $c_{i,\text{sat}}$ is the saturation loading, and n is the total number of species in mixture. An exceptional circumstance manifests for CO_2−CH_4, CO_2−Ar, and CO_2−N_2 mixture diffusion in LTA, DDR, and ERI zeolites; here the preferential location of CO_2 at the window regions serves to hinder the diffusion of partner molecules, lowering its diffusivity below the pure component value.[24,25] The diffusivity of CO_2 in the mixture remains unaffected by the partner species.

The second tenet is that the exchange coefficient $Đ_{12}$ can be estimated from the pure component self-exchange coefficients $Đ_{11}$ and $Đ_{22}$ using an interpolation formula.[10−18] One such interpolation formula is based on the Vignes[26] model for diffusion in liquid mixtures

$$Đ_{12} = (Đ_{11})^{x_1} (Đ_{22})^{x_2} \tag{8}$$

The two tenets have been verified on the basis of an extensive data set of molecular dynamics (MD) simulations for a variety of mixtures containing molecules such as alkanes, CO_2,CH_4, N_2, Ar, Ne, CF_4, and He in a wide variety of microporous structures such as zeolites, metal organic framework (MOFs), and carbon nanotubes (CNTs).[11−18] The foregoing set of equations form the basis for modeling adsorbers, reactors, and membrane permeation devices.[27−36]

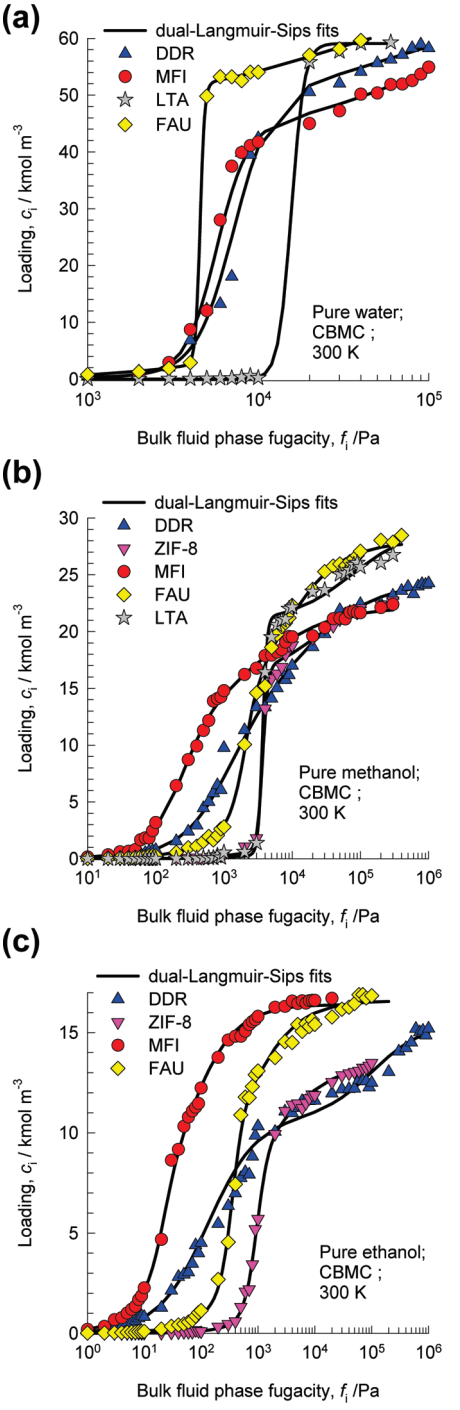

Figure 1. (a) CBMC simulations of adsorption isotherms for (a) water, (b) methanol, and (c) ethanol in LTA, FAU, MFI, DDR, and ZIF-8 at 300 K. Also shown with the continuous solid lines are the dual-Langmuir−Sips fits of the isotherms.

(21) Sanborn, M. J.; Snurr, R. Q. *Sep. Purif. Technol.* **2000**, *20*, 1–13.
(22) Dubbeldam, D.; Snurr, R. Q. *Mol. Simulation* **2007**, *33*, 15–30.
(23) Jobic, H.; Theodorou, D. N. *Microporous Mesoporous Mater.* **2006**, *102*, 21–50.
(24) Krishna, R.; van Baten, J. M. *Chem. Phys. Lett.* **2007**, *446*, 344–349.
(25) Krishna, R.; van Baten, J. M. *Sep. Purif. Technol.* **2008**, *61*, 414–423.
(26) Vignes, A. *Ind. Eng. Chem. Fundam.* **1966**, *5*, 189–199.
(27) Krishna, R.; Baur, R. *Sep. Purif. Technol.* **2003**, *33*, 213–254.
(28) van de Graaf, J. M.; Kapteijn, F.; Moulijn, J. A. *AIChE. J.* **1999**, *45*, 497–511.

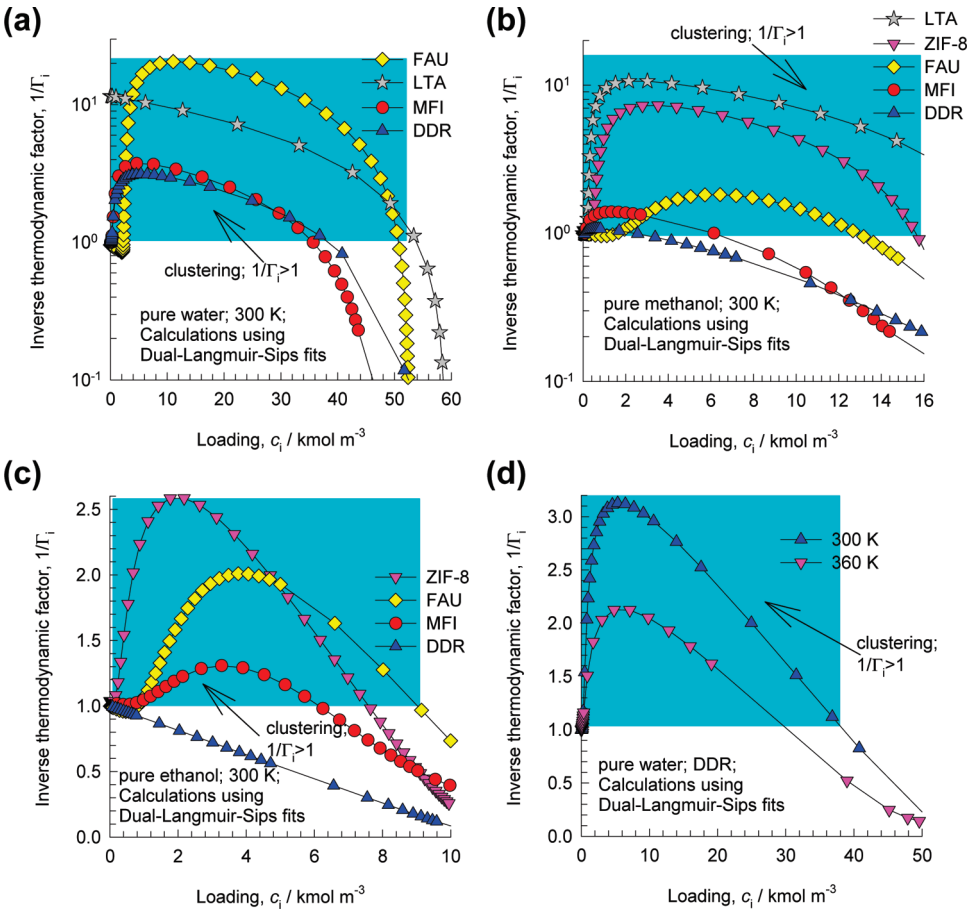

Figure 2. The inverse thermodynamic factor, $1/\Gamma_i$, plotted as a function of the pore loading, c_i for (a) water, (b) methanol, and (c) ethanol in LTA, FAU, MFI, DDR, and ZIF-8 at 300 K. The $1/\Gamma_i$ are calculated by differentiation of dual-Langmuir−Sips fits of the isotherms. (d) Comparison of $1/\Gamma_i$, for adsorption isotherms of water in DDR at 300 and 360 K.

For structures such as DDR, LTA, CHA, ERI, and ZIF-8 that consist of cages separated by narrow windows, correlation effects are often considered to be of negligible importance because only one molecule at a time can hop across from one cage to the neighboring one. This scenario can be expressed as

$$\frac{Đ_i}{Đ_{12}} \to 0; \quad i = 1, 2 \text{ (negligible correlations)} \qquad (9)$$

leading to a set of uncoupled equations, tantamount neglecting the cross-coefficients of [Δ]:

$$N_i = -\phi \frac{c_i}{RT} Đ_i \nabla \mu_i; \quad i = 1, 2 \text{ (negligible correlations)} \quad (10)$$

Equation 10 has been used with considerable success for modeling permeation of CO_2/CH_4, CH_4/N_2, CO_2/N_2, CO_2/Ar mixtures across CHA and DDR membranes.[31−33]

For water−alcohol mixture diffusion, there is some evidence in the literature to indicate mutual hindering effects. For water−ethanol permeation across an MFI membrane, Nomura et al.[37] found that the water permeance was seriously decreased by the presence of ethanol. For water−ethanol permeation across a DDR membrane, Kuhn et al.[6] found that both ethanol and water permeances decrease due to the presence of the partner species. For permeation of water−ethanol across a polydimethylsiloxane (PDMS) membrane, Nasiri et al.[38] found that the clustering of ethanol with water caused the diffusivities of both components to decrease below their respective pure component values. For permeation of water−methanol, and water−ethanol mixtures across a DDR membrane, the fluxes of water, methanol, and ethanol predicted by Kuhn et al.[7] with the uncoupled M−S eqs 10 are about an order of magnitude higher than those measured experimentally. Khajavi et al.[39] report experimental data on water−alcohol permeation across a SOD membrane. Their experiments show significant reduction in the water flux, by about 3 orders of magnitude, with increasing concentrations of secondary alcohols.

The main objective of this work is to demonstrate the pathological failure of both of the above-mentioned tenets when implementing the M−S equations to describe diffusion of water−alcohol mixtures in microporous materials. In order to develop the arguments leading to the above conclusions in a logical and systematic manner, we need to investigate pure component and

(29) Hansen, N.; Krishna, R.; van Baten, J. M.; Bell, A. T.; Keil, F. J. *J. Phys. Chem. C* **2009**, *113*, 235–246.
(30) Hansen, N.; Krishna, R.; van Baten, J. M.; Bell, A. T.; Keil, F. J. *Chem. Eng. Sci.* **2010**, *65*, 2472–2480.
(31) Li, S.; Falconer, J. L.; Noble, R. D.; Krishna, R. *J. Phys. Chem. C* **2007**, *111*, 5075–5082.
(32) Krishna, R.; van Baten, J. M.; García-Pérez, E.; Calero, S. *Ind. Eng. Chem. Res.* **2007**, *46*, 2974–2986.
(33) Krishna, R.; Li, S.; van Baten, J. M.; Falconer, J. L.; Noble, R. D. *Sep. Purif. Technol.* **2008**, *60*, 230–236.
(34) Ghoreyshi, A. A.; Farhadpour, F. A.; Soltanieh, M. *Chem. Eng. Commun.* **2004**, *191*, 460–499.
(35) Izak, P.; Bartovská, L.; Friess, K.; Šipek, M.; Uchytil, P. *J. Membr. Sci.* **2003**, *214*, 293–309.
(36) Lee, S. C. *J. Membr. Sci.* **2007**, *306*, 267–276.
(37) Nomura, M.; Yamaguchi, T.; Nakao, S. *J. Membr. Sci.* **1998**, *144*, 161–171.
(38) Nasiri, H.; Aroujalian, A. *Sep. Purif. Technol.* **2010**, *72*, 13–21.
(39) Khajavi, S.; Jansen, J. C.; Kapteijn, F. *J. Membr. Sci.* **2009**, *326*, 153–160.

mixture adsorption characteristics, along with a characterization of unary and mixture diffusion. For these purposes, we use Configurational-Bias Monte Carlo (CBMC) simulations of adsorption isotherms in the grand canonical ensemble, along with molecular dynamics (MD) simulations of diffusivities of pure components and mixtures. As guest molecules we choose water, methanol, and ethanol. As host structures we choose four zeolites: FAU, MFI, DDR, and LTA, that are relevant for use in pervaporation and dehydration applications. Additionally, we investigated the adsorption of methanol and ethanol in ZIF-8, that has a similar topology to that of SOD, in order to rationalize the recent experiments of Chmelik et al.[40] that have shown some peculiar unary diffusion characteristics.

The force field implementation for all-silica zeolites is the same as used in the Kuhn et al.[7] paper. The Lennard-Jones potentials for the framework atoms of ZIF-8 were taken from the combined works of Mayo et al.,[41] Yang and Zhong,[42] and Jorgensen et al.[43] as was reported in the computational study of Zhou et al.[44] The framework charges of ZIF-8 were estimated using the group-contribution procedure based on quantum mechanical calculations described in the recent paper by Xu and Zhong.[45]

The entire database of simulation results is available in the Supporting Information accompanying this publication; this material includes details of the CBMC and MD simulation methodologies, details of the microporous structures (unit cell dimensions, accessible pore volume, characteristic pore dimensions), pore landscapes, specification of the force fields used, simulation data on isotherms, clustering analysis, and diffusivities. Also presented are the explicit formulas for backing out the $Đ_1$, $Đ_2$, and $Đ_{12}$ from the MD simulated values Δ_{ij} for binary mixtures.

We start by investigating the adsorption characteristics of water and alcohols.

2. Pure Component and Mixture Adsorption

In recent years, there have been several molecular simulation and experimental studies on adsorption characteristics of water, methanol, and ethanol in a variety of microporous materials such as zeolites, metal−organic frameworks (MOFs), and carbon nanotubes. On the basis of these studies there is clear evidence of clustering of the polar guest molecules caused due to hydrogen bonding.[38,40,46−68] Because of cluster formation, the pure component adsorption isotherms of water and alcohols displays step-like

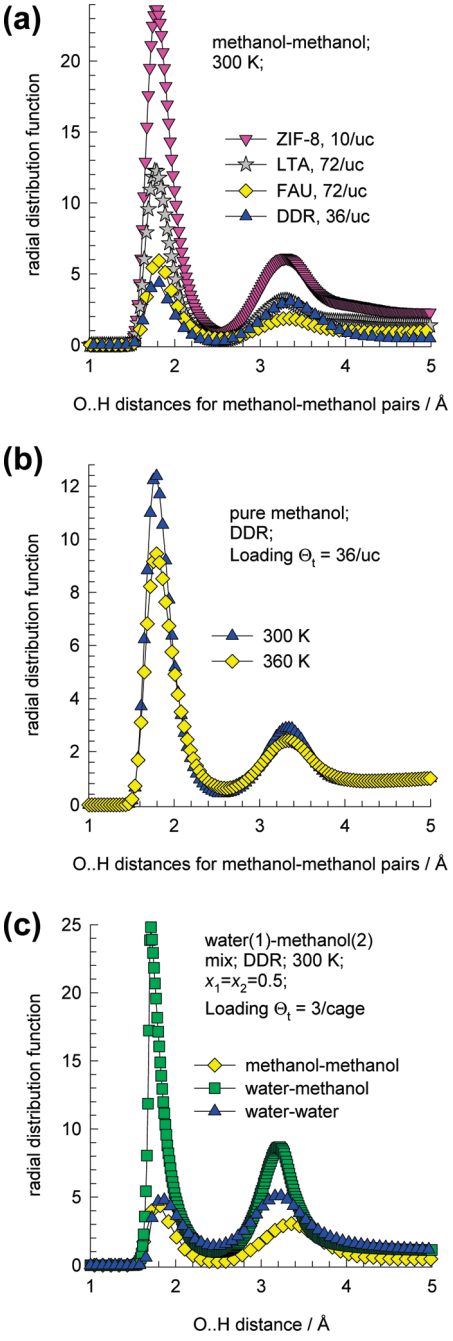

Figure 3. (a) Radial distribution functions (RDFs) for methanol-methanol molecular pairs in LTA, FAU, ZIF-8, and DDR at 300 K. The loadings per unit cell are 72, 72, 10, and 36 respectively. The RDFs are constructed on the basis of distances between the all intermolecular pairs of O and H atoms of methanol-methanol molecular pairs. (b) Comparison of RDFs for methanol-methanol molecular pairs in DDR at a total loading of 36 molecules per unit cell and at temperatures 300 and 360 K. (c) RDFs for an equimolar binary mixture of water and methanol in DDR at 300 K at a total loading of 36 molecules per unit cell, i.e., 3/cage.

(40) Chmelik, C.; Bux, H.; Caro, J.; Heinke, L.; Hibbe, F.; Titze, T.; Kärger, J. *Phys. Rev. Lett.* **2010**, *104*, 085902.
(41) Mayo, S. L.; Olafson, B. D.; Goddard, W. A. *J. Phys. Chem.* **1990**, *94*, 8897–8909.
(42) Yang, Q.; Zhong, C. *J. Phys. Chem. B* **2006**, *110*, 655–658.
(43) Jorgensen, W. L.; Maxwell, D. S.; Tirado-Rives, J. *J. Am. Chem. Soc.* **1996**, *118*, 11225–11236.
(44) Zhou, M.; Wang, Q.; Zhang, L.; Liu, Y. C.; Kang, Y. *J. Phys. Chem. B* **2009**, *113*, 11049–11053.
(45) Xu, Q.; Zhong, C. *J. Phys. Chem. C* **2010**, *114*, 5035–5042.
(46) Newalkar, B. L.; Jasra, R. V.; Kamath, V.; Bhat, S. G. T. *Microporous Mesoporous Mater.* **1998**, *20*, 129–137.
(47) Halasz, I.; Kim, S.; Marcus, B. *J. Phys. Chem. B* **2001**, *105*, 10788–10796.
(48) Bussai, C.; Fritzsche, S.; Haberlandt, R.; Hannongbua, S. *J. Phys. Chem. B* **2003**, *107*, 12444–12450.
(49) Demontis, P.; Stara, G.; Suffritti, G. B. *J. Phys. Chem. B* **2003**, *107*, 4426–4436.
(50) Demontis, P.; Gulin-González, J.; Jobic, H.; Masia, M.; Sale, R.; Suffritti, G. B. *ACS Nano* **2008**, *2*, 1603–1614.
(51) Demontis, P.; Jobic, H.; Gonzalez, M. A.; Suffritti, G. B. *J. Phys. Chem. C* **2009**, *113*, 12373–12379.
(52) Ari, M. U.; Ahunbay, M. G.; Yurtsever, M.; Erdem-Senatalar, A. *J. Phys. Chem. B* **2009**, *113*, 8073–8079.
(53) Plant, D. F.; Maurin, G.; Bell, R. G. *J. Phys. Chem. B* **2006**, *110*, 15926–15931.
(54) Yang, J. Z.; Liu, Q. L.; Wang, H. T. *J. Membr. Sci.* **2007**, *291*, 1–7.
(55) Yang, J. Z.; Chen, Y.; Zhu, A. M.; Liu, Q. L.; Wu, J. Y. *J. Membr. Sci.* **2008**, *318*, 327–333.
(56) Fleys, M.; Thompson, R. W.; MacDonald, J. C. *J. Phys. Chem. B* **2004**, *108*, 12197–12203.
(57) Fleys, M.; Thompson, R. W. *J. Chem. Theory Comput.* **2005**, *1*, 453–458.
(58) Di Lella, A.; Desbiens, N.; Boutin, A.; Demachy, I.; P., U.; Bellat, J. P.; Fuchs, A. H. *Phys. Chem. Chem. Phys.* **2006**, *8*, 5396–5406.
(59) Wu, J. Y.; Liu, Q. L.; Xiong, Y.; Zhu, A. M.; Chen, Y. *J. Phys. Chem. B* **2009**, *113*, 4267–4274.

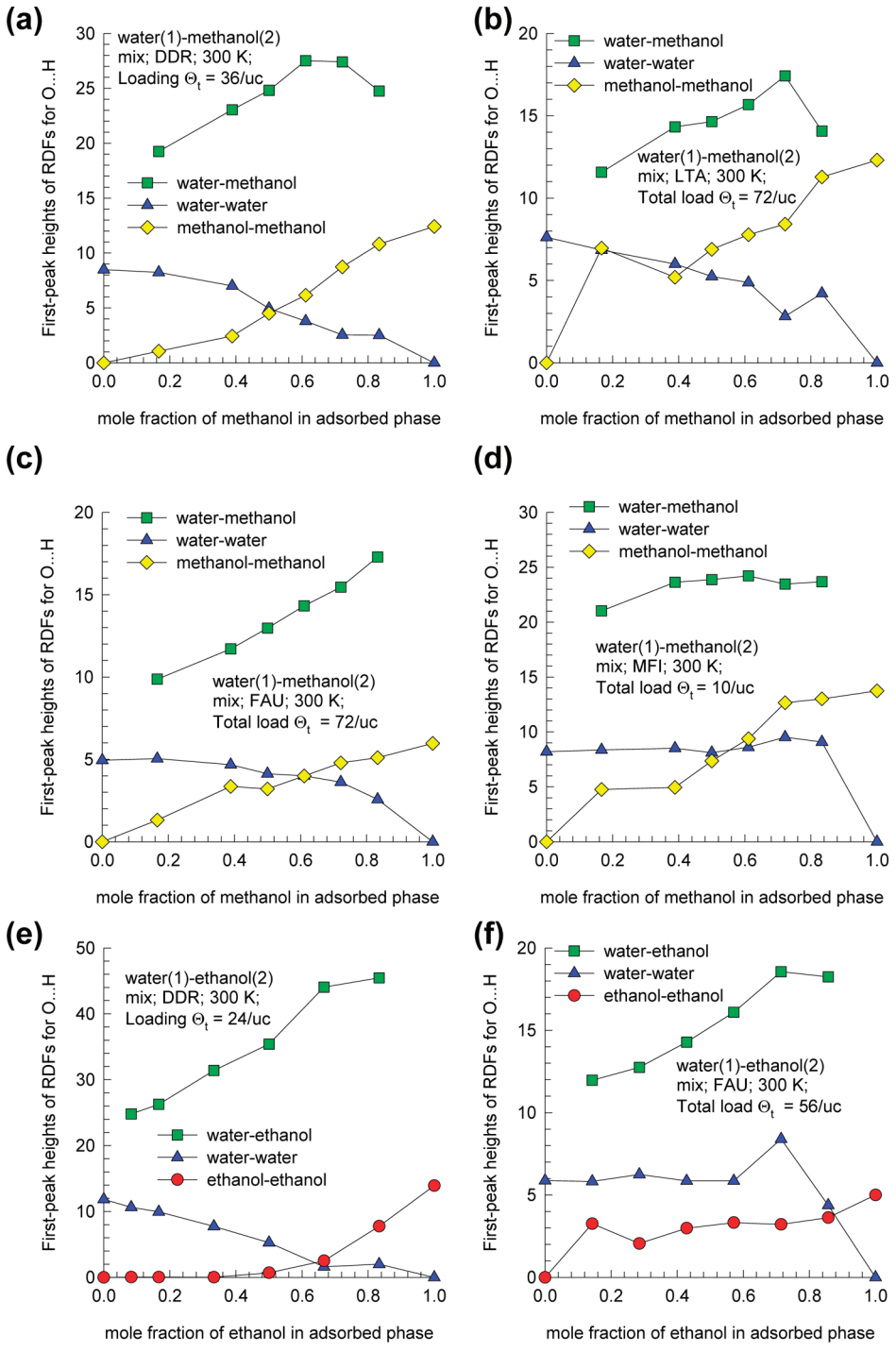

Figure 4. Plots of the first-peak heights of the RDFs, from data such as those presented in Figure 3, for water−methanol, and water−ethanol mixtures of varying composition in DDR, FAU, LTA, and MFI at 300 K.

characteristics.[40,46,47,57,58,62,64] To underline this, Figure 1 shows the CBMC simulations of pure component isotherms for water, methanol and ethanol in LTA, MFI, DDR, FAU, and ZIF-8 at 300 K. The c_i's are the absolute loadings, expressed as the number of moles per cubic meter of *accessible* pore volume; this allows a proper comparison of the loadings in different structures.[17,18,69−72] In this connection it must be noted that the sodalite cages of LTA, and FAU are inaccessible and need to be blocked in simulations.[73]

(60) Konduri, S.; Tong, H. M.; Chempath, S.; Nair, S. *J. Phys. Chem. C* **2008**, *112*, 15367–15374.
(61) Yazaydın, A. Ö.; Thompson, R. W. *Microporous Mesoporous Mater.* **2009**, *123*, 169–176.
(62) Narasimhan, L.; Boulet, P.; Kuchta, B.; Schaef, O.; Denoyel, R.; Brunet, P. *Langmuir* **2009**, *25*, 11598–11607.
(63) Nanok, T.; Vasenkov, S.; Keil, F.; Fritzsche, S. *Microporous Mesoporous Mater.* **2010**, *127*, 176–181.
(64) Pillai, R. S.; Jasra, R. V. *Langmuir* **2010**, *26*, 1755–1764.
(65) Lu, L.; Shao, Q.; Huang, L.; Lu, X. *Fluid Phase Equilib.* **2007**, *261*, 191–198.
(66) Puibasset, J.; Pellenq, R. J. M. *J. Phys. Chem. B* **2008**, *112*, 6390–6397.
(67) Zang, J.; Konduri, S.; Nair, S.; Sholl, D. S. *ACS Nano* **2010**, *3*, 1548–1556.
(68) Zang, J.; Chempath, S.; Konduri, S.; Nair, S.; Sholl, D. S. *J. Phys. Chem. Lett.* **2010**, *1*, 1235–1240.
(69) Babarao, R.; Tong, Y. H.; Jiang, J. *J. Phys. Chem. B* **2009**, *113*, 9129–9136.
(70) Krishna, R.; van Baten, J. M. *Chem. Eng. Sci.* **2009**, *64*, 870–882.
(71) Krishna, R.; van Baten, J. M. *Langmuir* **2010**, *26*, 3981–3992.
(72) Krishna, R.; van Baten, J. M. *Langmuir* **2010**, http://dx.doi.org/10.1021/la904895y.

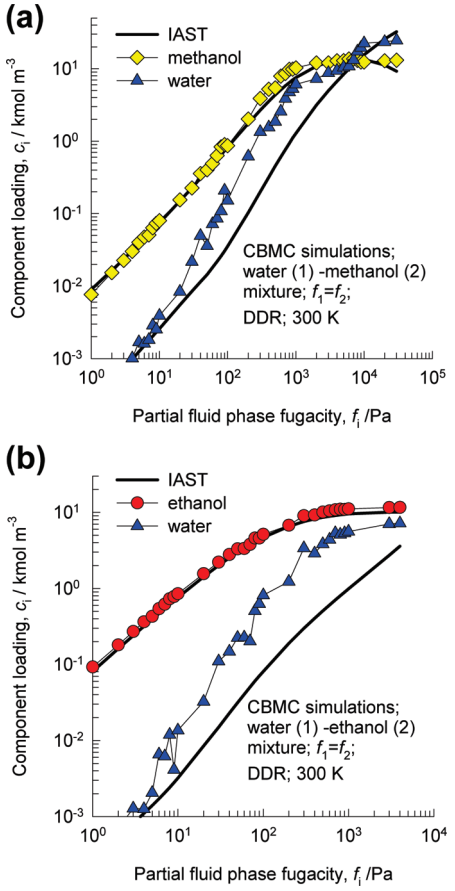

Figure 5. CBMC simulations of component loadings of (a) water (1) and methanol (2) and (b) water (1) and ethanol (2), mixtures in DDR at 300 K, as a function of the partial fluid phase fugacity f_i. The partial fugacities in the bulk fluid phase of the components are taken to be equal, i.e. $f_1 = f_2$. The continuous solid lines represent the calculations using the ideal adsorbed solution theory (IAST) of Myers and Prausnitz,[79] using the pure component isotherm fits as data inputs.

Also, DDR contains pockets that are inaccessible; these pockets need to be blocked in Monte Carlo simulations.[73] In the simulations presented by Kuhn et al.[7] for DDR zeolite, the inaccessible pockets were not blocked and their original simulation results are incorrect. This error was acknowledged and a correction was published subsequently.[74] The accessible pore volumes of the variety of structures investigated were determined with the aid of molecular simulations using the helium probe insertion technique suggested by Talu and Myers.[75,76] The continuous solid lines in Figure 1 are fits using the dual-Langmuir−Sips isotherm:[71,72,77]

$$c_i = c_{i,A,sat}\frac{b_{i,A}f_i^{\nu_{i,A}}}{1+b_{i,A}f_i^{\nu_{i,A}}} + c_{i,B,sat}\frac{b_{i,B}f_i^{\nu_{i,B}}}{1+b_{i,B}f_i^{\nu_{i,B}}} \qquad (11)$$

All the six constants in eq 11 were fitted to match the CBMC simulated isotherms; neither exponent $\nu_{i,A}$ and $\nu_{i,B}$ was restricted to unity. The inverse thermodynamic factor, $1/\Gamma_i$, defined by

$$\frac{1}{\Gamma_i} \equiv \frac{\partial[\ln c_i]}{\partial[\ln f_i]} = \frac{f_i}{c_i}\frac{\partial c_i}{\partial f_i} \qquad (12)$$

can be obtained by analytic differentiation of eq 11. The data for $1/\Gamma_i$ are presented in Figure 2. We prefer to plot $1/\Gamma_i$ instead of Γ_i because the latter has the undesirable property of approaching infinity as saturation loading is approached; this makes the data less easy to interpret when plotted in graphical form. For a single-site Langmuir isotherm, we have $1/\Gamma_i = (1 - \theta_i) = (1 - c_i/c_{i,sat})$, i.e. the fractional vacancy. In previous work we had argued that the condition $1/\Gamma_i > 1$ implies the increase of fractional vacancy beyond unity and this is physically rationalized if we allow for molecular clustering.[71,72] We note from Figure 2 that $1/\Gamma_i$ exceeds unity for most guest−host combinations. The volumes of each cage of ZIF-8, FAU, LTA, and DDR, from pore volume determinations,[71] are 1168, 786, 743, and 278 Å^3, respectively. Broadly speaking, the degree of clustering increases with cage capacity, because the propensity to form clusters increases as the number of neighboring molecules inside a cage increases. The recent experimental data of Chmelik et al.[40] for methanol and ethanol adsorption in ZIF-8 provide confirmation of the significant increase of $1/\Gamma_i$ beyond unity values. For DDR, the $1/\Gamma_i$ for methanol and ethanol barely exceeds unity because for these molecules the number of molecules per cage, even under at saturation loadings, is 4 and 2.5 molecules per cage, respectively.

Increasing temperature, T, decreases the extent of clustering and this gets reflected in a reduction in the extent to which $1/\Gamma_i$ exceeds unity. To illustrate this we compare the $1/\Gamma_i$ data for water in DDR at 300 and 360 K in Figure 2d.

To demonstrate that the cause of molecular clustering is the hydrogen bonding between molecular pairs, we determined the radial distribution functions (RDFs) for distances between all combinations of O and H atoms of molecule pairs. As an example, the data for methanol−methanol pairs is presented in Figure 3a for LTA, FAU, DDR, and ZIF-8. We note the first peaks in the RDFs occur at a distance less than 2 Å, that is characteristic of hydrogen bonding.[78]

Figure 3b compares the RDFs for DDR at 300 and 360 K. Increasing the temperature decreases the height of the first peak of the RDF, indicating a lower degree of hydrogen bonding. This result is consonant with those presented for $1/\Gamma_i$ in Figure 2d.

We also determined the RDFs for water−methanol and water−ethanol mixtures of varying composition in all four zeolites. Figure 3c presents typical results for the RDFs obtained an equimolar mixture in DDR for each of the three molecular pairs: water−water, methanol-methanol, and water−methanol. It is clear that hydrogen bonding manifests for all three pairs because the first peaks occur at distances smaller than 2 Å in all three cases. Furthermore, we note that the first peak value is significantly higher for the water−methanol pair, indicating that clustering between these two pairs is the strongest.

The degree of molecular clustering due to hydrogen bonding can be characterized by the magnitudes of the first peaks.[78] Collecting the data on the magnitude of the first peaks for water−alcohol mixtures in the four zeolites, we prepared plots of the first-peak heights as a function of the alcohols fraction; see Figure 4.

There are important consequences of water−alcohol clustering on mixture adsorption. To underline this parts a and b of Figure 5 present CBMC simulations of the component loading for adsorption of water−methanol and water−ethanol mixtures in DDR at 300 K. The continuous solid lines in Figure 5 are the estimations

(73) Krishna, R.; van Baten, J. M. *Langmuir* **2010**, *26*, 2975–2978.
(74) Kuhn, J.; Castillo-Sanchez, J. M.; Gascon, J.; Calero, S.; Dubbeldam, D.; Vlugt, T. J. H.; Kapteijn, F.; Gross, J. *J. Phys. Chem. C* **2010**, *114*, 6877–6878.
(75) Talu, O.; Myers, A. L. *AIChE. J.* **2001**, *47*, 1160–1168.
(76) Myers, A. L.; Monson, P. A. *Langmuir* **2002**, *18*, 10261–10273.
(77) Chmelik, C.; Kärger, J.; Wiebcke, M.; Caro, J.; van Baten, J. M.; Krishna, R. *Microporous Mesoporous Mater.* **2009**, *117*, 22–32.
(78) Zhang, C.; Yang, X. *Fluid Phase Equilib.* **2005**, *231*, 1–10.

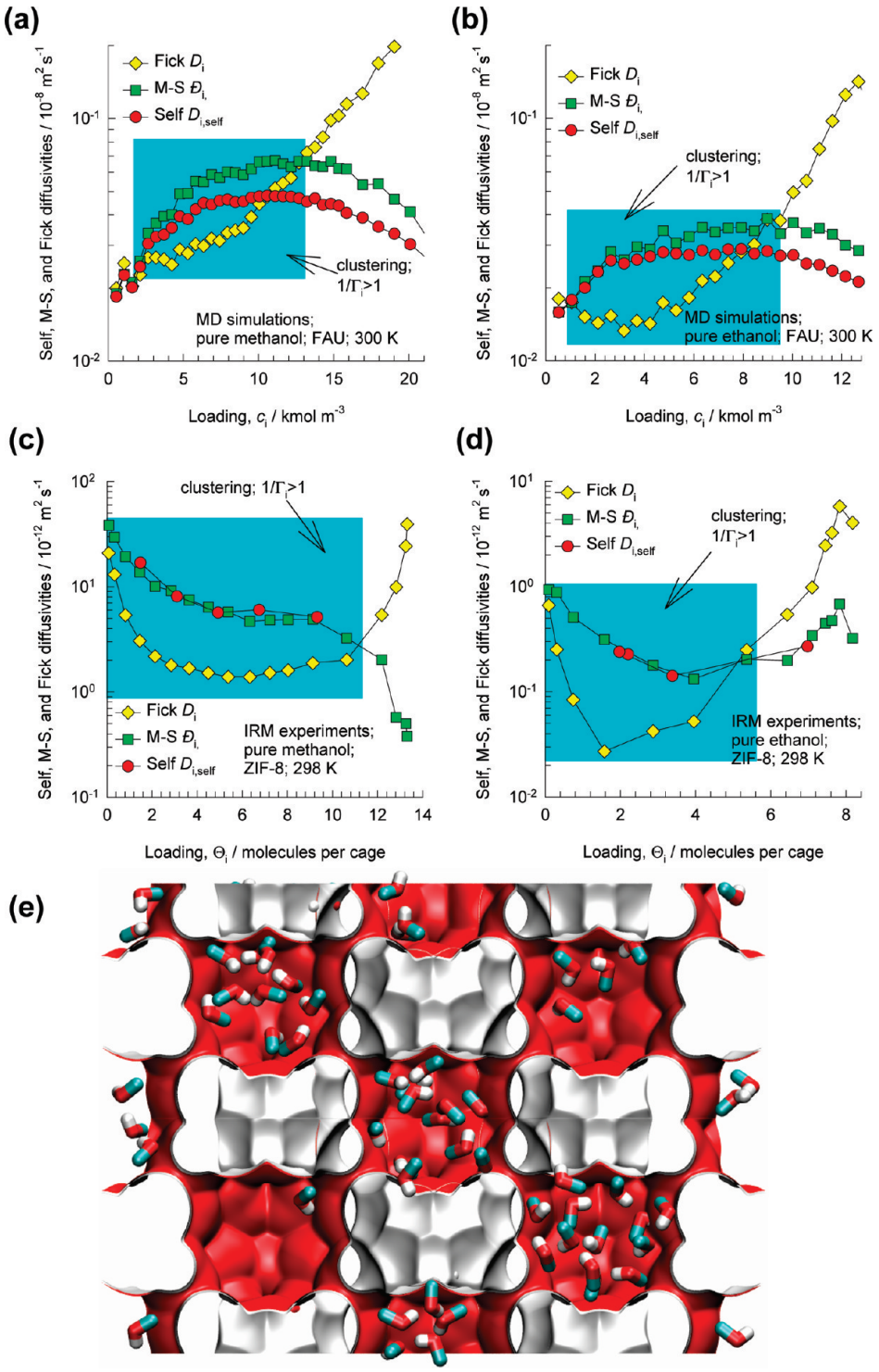

Figure 6. (a, b) MD simulation results for the loading dependences of the Maxwell−Stefan (M−S) diffusivity, $Đ_i$, Fick diffusivity, D_i, and the self-diffusivity, $D_{i,self}$ for (a) methanol, and (b) ethanol in FAU at 300 K. (c, d) Experimental data of Chmelik et al.[40] for $Đ_i$, D_i, and $D_{i,self}$ for (c) methanol, and (d) ethanol obtained by Infrared microscopy and infrared microimaging (IRM). The original IRM data is expressed in terms of fractional loadings. These loadings have been converted to loadings in molecules per cage, by comparing the IRM isotherms with the CBMC simulated data shown in Figure 1; see also Supporting Information for further details. The shaded areas represent the concentration regions for which $1/\Gamma_i > 1$; these correspond to those in Figure 2. (e) Snapshot showing the equilibrium positions of adsorbed methanol molecules in ZIF-8.

of the ideal adsorbed solution theory (IAST) of Myers and Prausnitz,[79] using the pure component dual-Langmuir−Sips isotherm fits as data inputs. The IAST assumes a homogeneous distribution of components within the pore space, and does not account for the significant water−alcohol clusters formed by hydrogen bonding. The clustering of water molecules around methanol serves to effectively enhance its adsorption strength, exceeding the value predicted by the IAST. There is also evidence

(79) Myers, A. L.; Prausnitz, J. M. *AIChE. J.* **1965**, *11*, 121–130.

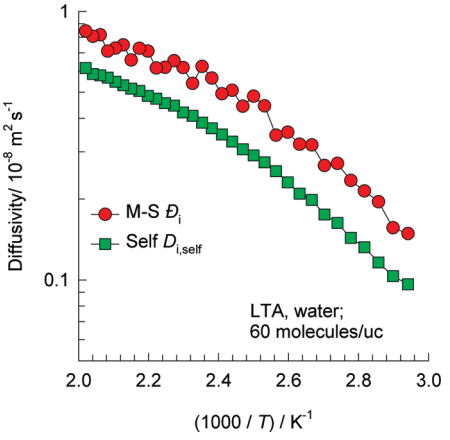

Figure 7. Arrhenius plots for MD simulated values of self-diffusivity $D_{i,self}$ and M−S diffusivity $Đ_i$ of water in LTA for a loading of 60 molecules per unit cell, corresponding to c_i = 16.76 kmol m^{-3}.

suggesting the failure of IAST for water−methanol adsorption in single walled aluminosilicate nanotubes.[68] Analogous results are obtained for mixture adsorption in FAU; see Supporting Information.

A visual, albeit qualitative, appreciation of the clustering induced by hydrogen bonding can be obtained by viewing the animations of MD simulations of water, methanol, ethanol, water−methanol, and water−ethanol diffusion in DDR, LTA, and ZIF-8; these movies are provided as Supporting Information.

3. Influence of Molecular Clustering on Unary Diffusion

When no molecular clustering occurs, $1/\Gamma_i < 1$, the hierarchy Fick D_i > M−S $Đ_i$ > self-diffusivity $D_{i,self}$, prevailing over the concentration range; this typifies "normal" behavior for guest molecules in microporous structures. In regions where $1/\Gamma_i > 1$, the Fick diffusivity D_i is often lower than either the M−S diffusivity $Đ_i$ or the self-diffusivity, $D_{i,self}$; this is illustrated by the MD simulation results in Figures 6a and 6b for methanol and ethanol diffusion in FAU. The shaded areas represent the concentration regions for which $1/\Gamma_i > 1$; these correspond to those in Figure 2. Analogous results are obtained for other guest−host combinations; see Supporting Information. A further point to note in Figure 6 is the maxima in the loading dependence of the M−S and self-diffusivities for methanol and ethanol in FAU. Our MD results provide a theoretical background to the maximum in the loading dependence of the self-diffusivity of methanol in NaX zeolite found in the experimental investigation of Brandani et al.[80] A similar maximum in the diffusivity of CH_4 in NaY zeolite at subcritical temperatures was observed in MD simulations.[71,72] This behavior is caused due to molecular clustering that occurs at $T < T_c$ and more recently published QENS experiments provide experimental confirmation of this trend.[81]

Direct experimental verification of $D_i < D_{i,self}$ when $1/\Gamma_i > 1$ is available in the recent work of Chmelik et al.[40] for methanol and ethanol diffusion in ZIF-8; see Figures 6c and 6d. One practical consequence of the decrease in the Fick D_i with increasing c_i is that the desorption kinetics may be expected to be higher than the adsorption kinetics, i.e. opposite to that commonly observed in practice.[27,82] A visual appreciation of methanol clustering is provided in Figure 6e which presents snapshots of the location of adsorbed methanol molecules in ZIF-8. Besides forming clusters, it is apparent from this snapshot that there is also a tendency for molecules to congregate, leading to unequal cage occupancies.

A further remarkable aspect of the experimental data of Chmelik et al.[40] concerns the loading dependence of the M−S diffusivities, $Đ_i$. ZIF-8 has a topology similar to SOD zeolite, and consists of 1168 Å^3 cages, separated by narrow 3.4 Å sized windows. For structures such as LTA, ITQ-29, CHA, DDR, and SOD, the loading dependence of $Đ_i$ is characterized by a pronounced maximum for nonpolar guest molecules such as CH_4. The increase in $Đ_i$ for concentrations below the maximum is to be attributed to a decreases in the free energy barrier for intercage hopping.[83,84] The deviant behavior of methanol and ethanol in ZIF-8, with a decrease of $Đ_i$ is most likely due to an strong increase in the free energy barrier for intercage hopping. This aspect deserves further attention.

Figure 7 presents the Arrhenius plots for both $D_{i,self}$ and $Đ_i$ of water in LTA at a total loading of 60 molecules per unit cell, corresponding to c_i = 16.76 kmol m^{-3}. Because of severe water clustering, the T-dependence of both diffusivities display non-Arrhenius characteristics. The MD simulation results of Fleys et al.[56] show similar non-Arrhenius behaviors of diffusivities of water in silicalite and DAY, also caused by cluster formation.

4. Influence of Clustering on Mixture Diffusion

For water−methanol and water−ethanol mixtures, several MD campaigns were carried out to determine the M−S coefficients $Đ_1$, $Đ_2$, and $Đ_{12}$. in FAU, MFI, DDR, and LTA. Consider first the MD simulations results for equimolar ($c_1 = c_2$) water−methanol and water−ethanol mixtures in FAU; see Figure 8, parts a and b. The M−S diffusivity, $Đ_i$, of either component is lower than the corresponding pure component values when compared at the total occupancy θ_t, evaluated using eq 7 with saturation capacities determined from the CBMC simulated isotherms. These results are dramatically different from those for nonpolar mixtures for which it is commonly found that the $Đ_i$ retains the same value in the mixture.[11−18] The first tenet in using the M−S equations is clearly violated for FAU.

Let us now examine the validity of the second tenet, namely that the correlations in binary mixtures can be estimated on the basis of data on correlations of the constituent pure component say by use of the Vignes interpolation formula 8. For diffusion of water−methanol and water−ethanol mixtures in FAU, the data on $Đ_{11}$, $Đ_{22}$, and $Đ_{12}$ are presented in Figure 8, parts c and d. For equimolar mixtures, we see that the $Đ_{12}$ is about an order of magnitude lower than the pure component $Đ_{ii}$. Mixture diffusion is much more strongly correlated than for the pure constituents, and interpolation leads to erroneous predictions.

A different perspective of the special features of water−alcohol diffusion is obtained by considering the influence of varying mixture composition at a constant total loading, c_t; see data for both $Đ_i$, and the $Đ_{12}$, presented in Figure 9 for FAU. The addition of alcohol causes a dramatic reduction in the M−S diffusivity of water molecules in all cases. The reason for this can be traced to the fact that water molecules have the propensity to form hydrogen bonds with alcohol molecules; this cluster formation has

(80) Brandani, S.; Ruthven, D. M.; Kärger, J. *Zeolites* **1995**, *15*, 494–495.
(81) Déroche, I.; Maurin, G.; Borah, B. J.; Jobic, H.; Yashonath, S. *J. Phys. Chem. C* **2010**, *114*, 5027–5034.
(82) Garg, D. R.; Ruthven, D. M. *Chem. Eng. Sci.* **1972**, *27*, 417–423.
(83) Beerdsen, E.; Dubbeldam, D.; Smit, B. *J. Phys. Chem. B* **2006**, *110*, 22754–22772.
(84) Beerdsen, E.; Dubbeldam, D.; Smit, B. *Phys. Rev. Lett.* **2006**, *96*, 044501.

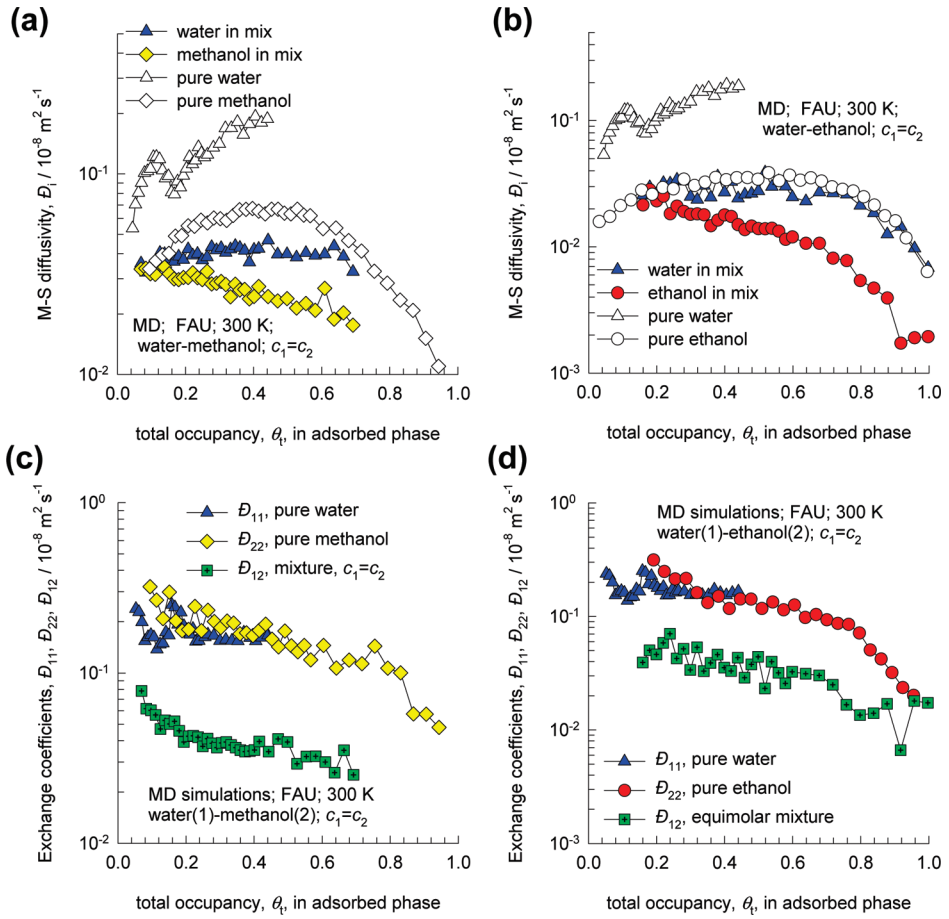

Figure 8. MD simulations of (a, b) M−S diffusivities, $Đ_i$, and (c, d) binary exchange coefficients, $Đ_{12}$, for diffusion of water−methanol and water−ethanol mixtures in FAU at 300 K. The data are for equimolar ($c_1 = c_2$) mixtures. Also shown are the data for unary diffusion, at the same total occupancy as in the mixture, θ_t. The fractional occupancies are calculated using the saturation capacities determined from pure component CBMC simulated isotherms. The values thus obtained are $c_{i,sat}$ = 60, 28, and 17 kmol m^{-3} for water, methanol, and ethanol, respectively.

the net effect of reducing its mobility. Another remarkable observation is the minimum in the alcohol diffusivities at a certain mixture composition. A similar minimum also manifests for diffusivities in the water−alcohol mixtures.[78,85,86]

The variation of the exchange coefficient $Đ_{12}$ with mixture composition shows a pronounced minimum; see Figures 9c, and 9d. Except for dilute mixtures, we note that the Vignes interpolation formula 8 leads to significant overestimation of $Đ_{12}$. This type of composition dependence is pathological for the M−S diffusivity $Đ_{12}$ in water−alcohol *fluid* mixtures exhibiting strong thermodynamic nonidealities.[87−91] In order to demonstrate this we carried out MD simulations to determine the M−S diffusivity $Đ_{12}$ in water−methanol and water−ethanol mixtures. The total mixture concentration was held constant at c_t = 11.7 kmol m^{-3}, and the compositions were varied. The results are presented in Figures 9e, and 9f. It can be observed that the Vignes interpolation formula overpredicts $Đ_{12}$ to a significant extent at intermediate compositions. This failure of the Vignes formula is traceable to the strong water−alcohol hydrogen bonding, as evidenced by the first-peak heights in Figure 4.

The data on $Đ_i$ in MFI for water−methanol mixtures of varying composition are shown in Figure 10a. We see a dramatic reduction in the water diffusivity with increasing composition of methanol but the diffusivity of methanol is only slightly reduced due to the presence of water. These data provide a rationale for the experimental finding of Nomura et al.[37] that the water permeance across an MFI membrane was significantly decreased by the presence of ethanol. The corresponding influence on ethanol was, however, found to be negligible. Yu et al.[92] found that their experimental data on permeation of methanol-acetone mixtures across an MFI membrane can only be rationalized if both the component $Đ_i$, are lowered in the mixture, when compared with the pure component values. The underlying cause of their findings is most likely to be due to the clustering caused by hydrogen bonding of acetone and methanol molecules, and evidence of such clustering is provided by molecular simulations.[93] Figure 10b underlines the failure of the Vignes interpolation formula 8 for estimation of the $Đ_{12}$ in MFI.

Let us now consider the composition dependence of the self-diffusivities, $Đ_{i,self}$, of binary mixtures. Starting with M−S

(85) Ferrario, M.; Haughney, M.; McDonald, I. R.; Klein, M. L. *J. Chem. Phys.* **1960**, *93*, 5156–5166.
(86) Zhang, L.; Wang, Q.; Liu, Y. C.; Zhang, L. Z. *J. Chem. Phys.* **2006**, *125*, 104502.
(87) Anderson, D. K.; Hall, J. R.; Babb, A. L. *J. Phys. Chem.* **1958**, *62*, 404–408.
(88) Clark, W. M.; Rowley, R. L. *AIChE. J.* **1986**, *32*, 1125–1131.
(89) Lee, Y. E.; Li, S. F. Y. *J. Chem. Eng. Data* **1991**, *36*, 240–243.
(90) Derlacki, Z. J.; Easteal, A. J.; Edge, A. V. J.; Woolf, L. A.; Roksandic, Z. *J. Phys. Chem.* **1995**, *89*, 5318–5322.
(91) Krishna, R.; van Baten, J. M. *Chem. Eng. Technol.* **2006**, *29*, 516–519.
(92) Yu, M.; Falconer, J. L.; Noble, R. D.; Krishna, R. *J. Membr. Sci.* **2007**, *293*, 167–173.
(93) Jia, Y.; Guo, X. *Chin. J. Chem. Eng.* **2006**, *14*, 413–418.

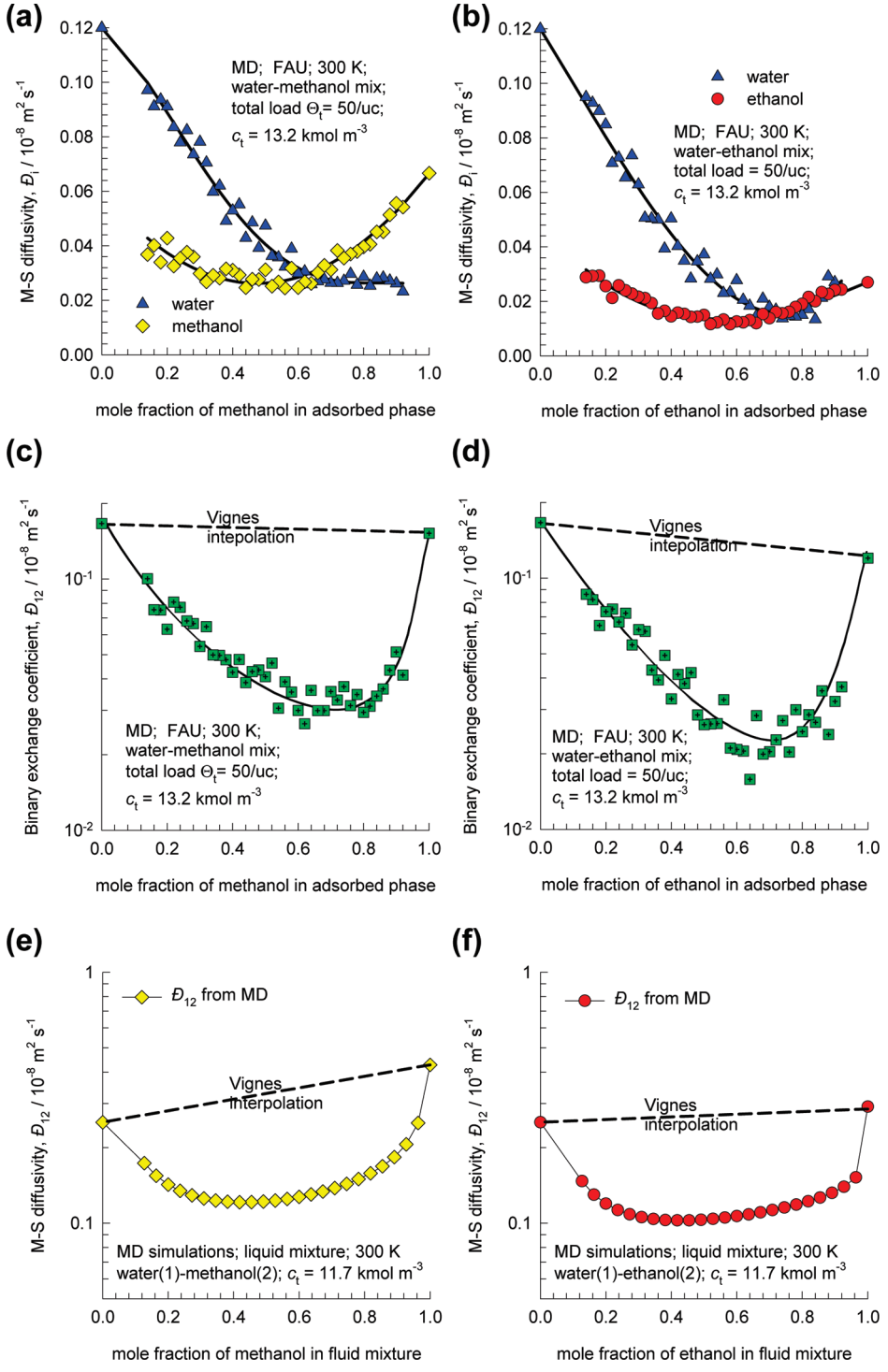

Figure 9. MD simulations of (a, b) M−S diffusivities, $Đ_i$, and (c, d) binary exchange coefficients, $Đ_{12}$, for diffusion of water−methanol and water−ethanol mixtures in FAU at 300 K. The data were obtained a total loading of 50 molecules per unit cell, corresponding to c_t = 13.2 kmol m^{-3}. Maxwell−Stefan diffusivities, $Đ_{12}$, for (e) water−methanol and (f) water−ethanol mixtures in a fluid mixture at a total concentration c_t = 11.7 kmol m^{-3}. The dashed lines in parts c−f represent calculations using the Vignes interpolation formula 8.

equations eq 1, the following relations for the $D_{i,self}$ can be derived[18]

$$D_{1,self} = \left(\frac{1}{Đ_1} + \frac{x_2}{Đ_{12}} + \frac{x_1}{Đ_{11}}\right);$$
$$D_{2,self} = \left(\frac{1}{Đ_2} + \frac{x_1}{Đ_{12}} + \frac{x_2}{Đ_{22}}\right) \qquad (13)$$

Correlation effects, encapsulated in the $Đ_{11}$, $Đ_{22}$, and $Đ_{12}$, normally have the effect of reducing the self-diffusivity of the more mobile species, while concomitantly enhancing that of the tardier partner. For water−alcohol mixtures the variation of $D_{i,self}$ with mixture composition is much more complex than for nonpolar mixtures. First, the pure component $Đ_i$ of both components are influenced by partner molecules, due to mutual hindering. Additionally, the correlation effects in the mixture are stronger than for either of the pure components. A combination

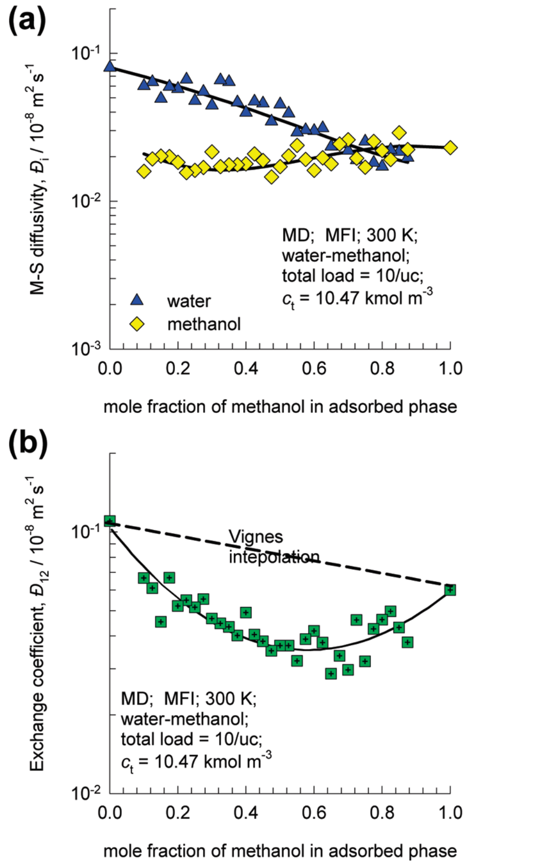

Figure 10. MD simulations of (a) M−S diffusivities, $Đ_i$, and (b) binary exchange coefficients, $Đ_{12}$, for diffusion of water−methanol mixtures in MFI at 300 K. The data for MFI were obtained a total loading of 10 molecules per unit cell, corresponding to c_t = 10.47 kmol m^{-3}. The dashed line in part b represents calculations using the Vignes interpolation formula 8.

of these two effects may be expected to lead to a much stronger composition dependence of the $D_{i,self}$ than observed earlier for the $Đ_i$ alone. Indeed, the alcohol self-diffusivities $D_{i,self}$ in FAU show pronounced minima; see Figure 11, parts a and b. The self-diffusivities of water−methanol mixtures in single walled aluminosilicate nanotubes[67] show characteristics that are similar to that in FAU. The minima are caused by a balance between two opposing factors: (1) increased mutual hindering, which has a tendency to reduce the $Đ_i$, and (2) increased correlations, which have a tendency to bring the mobilities of the two species closer to each other. The minima in the self-diffusivities are reminiscent of those experimentally observed for tracer diffusion in water−alcohol liquid mixtures.[90,94] MD simulations for $D_{i,self}$ in water−alcohol liquid mixtures have established that the root cause of the minima lies in the strong hydrogen bonding characteristics between water and alcohol molecules.[78,85,86]

For MFI, the methanol self-diffusivity is practically independent of composition, while that for water shows a dramatic decrease with increasing methanol concentration; see Figure 11c. The NMR experimental data of Caro et al.[95] on self-diffusivities of water−methanol mixtures in silcalite-1, and HZSM-5 provide direct confirmation of this trend.

A different perspective on the peculiarities of water−alcohols diffusion is obtained by considering the ratio of the self-diffusivity

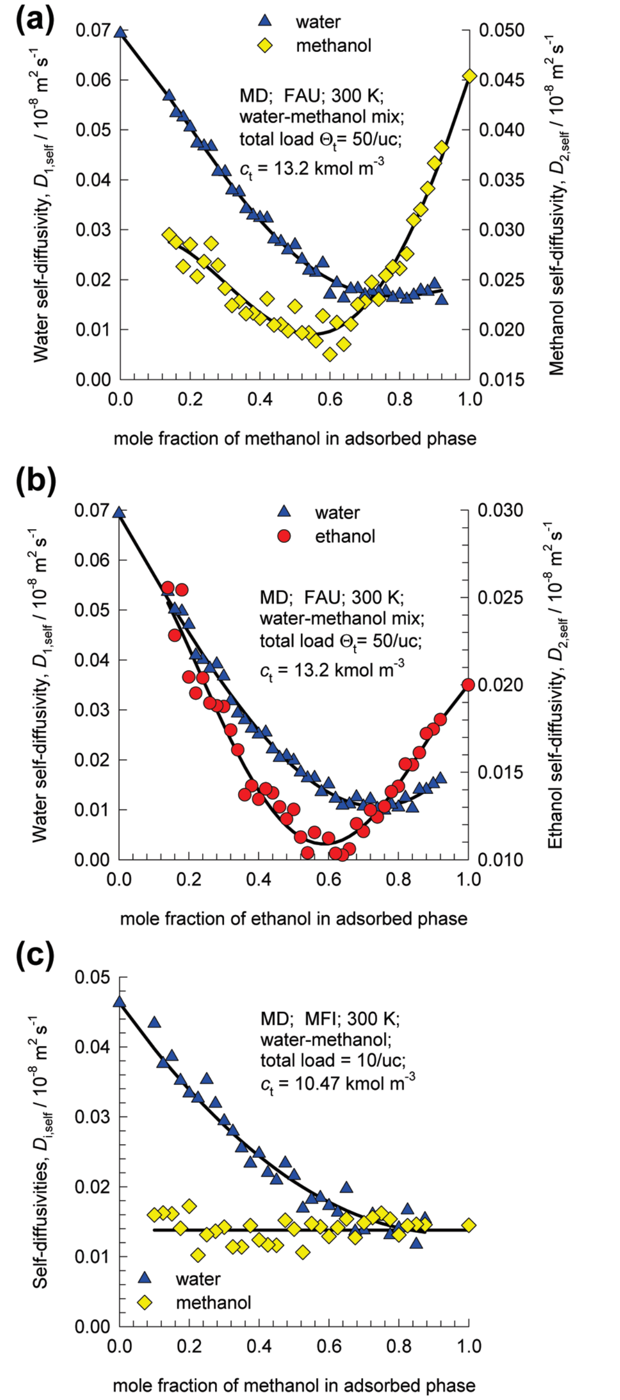

Figure 11. Self-diffusivities, $D_{i,self}$, in water−alcohol mixtures of varying composition, and constant total mixture loading c_t. Key: (a) water−methanol in FAU, (b) water−ethanol in FAU, and (c) water−methanol in MFI.

of alcohol to that of water; see Figure 12a. For both FAU and MFI, increasing methanol concentration increases the ratio of diffusivity of methanol with respect to water. This trend is exactly opposite to that for nonpolar mixtures for which increasing the proportion of the tardier species in the mixture decreases this ratio. Also shown in Figure 12a are the data for a liquid mixture at approximately the same total molar loading c_t as within the pores of FAU and MFI; the same increasing trend is observed, emphasizing the notion that the peculiarities stem from molecule−molecule interactions and intermolecular hydrogen bonding, rather than due to interactions with the framework. A further point to note is that this increasing

(94) Harris, K. R.; Newitt, P. J.; Derlacki, Z. J. *J. Chem. Soc., Faraday Trans* **1998**, *94*, 1963–1970.
(95) Caro, J.; Bülow, M.; Richter-Mendau, J.; Kärger, J.; Hunger, M.; Freude, D. *J. Chem. Soc., Faraday Trans.* **1987**, *83*, 1843–1849.

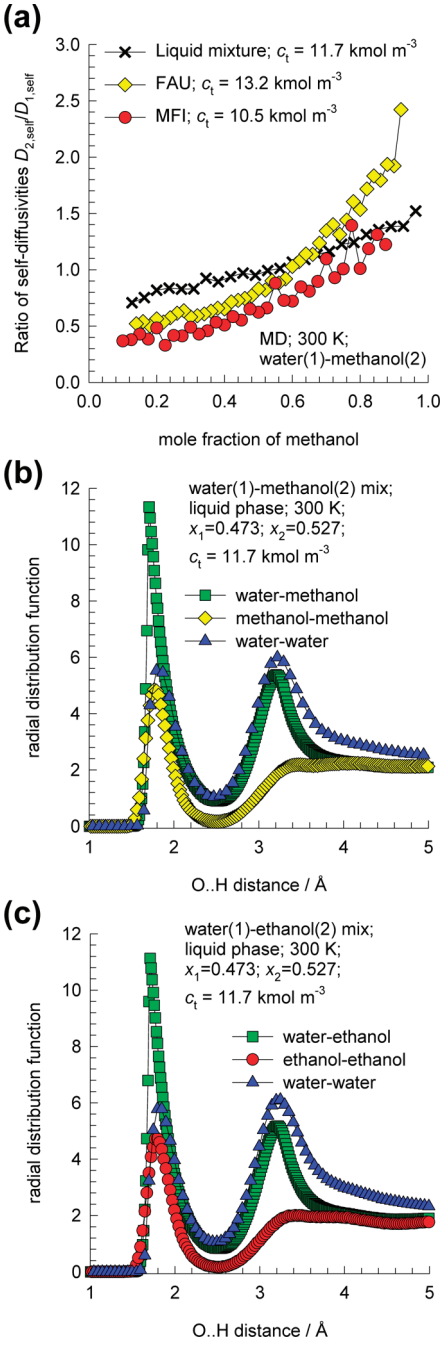

Figure 12. (a) Ratio of self-diffusivity of methanol to that of water, $D_{2,self}/D_{1,self}$, for water(1)−methanol(2) diffusion in FAU, and MFI at 300 K. Also shown is the data of MD simulations for water(1)−methanol(2) liquid mixture. (b) RDFs for binary liquid mixture of water and methanol at 300 K at a total concentration c_t = 11.7 kmol m^{-3}. (c) RDFs for binary liquid mixture of water and ethanol at 300 K at c_t = 11.7 kmol m^{-3}.

trend in the diffusivity ratio is directly related to the increase in the extent of hydrogen-bonding between water and methanol molecules; see first-peak heights in Figure 4.

The RDFs for O−H bond distances for binary water−methanol and water−ethanol mixtures are shown in Figure 12, parts b and c. As is the case within micropores, the water−alcohol peak values are the highest. These RDFs provide an explanation for the failure of the Vignes interpolation formula for liquid mixtures (cf. Figure 9, parts e and f), and can be traced to much stronger water−alcohol bonding.

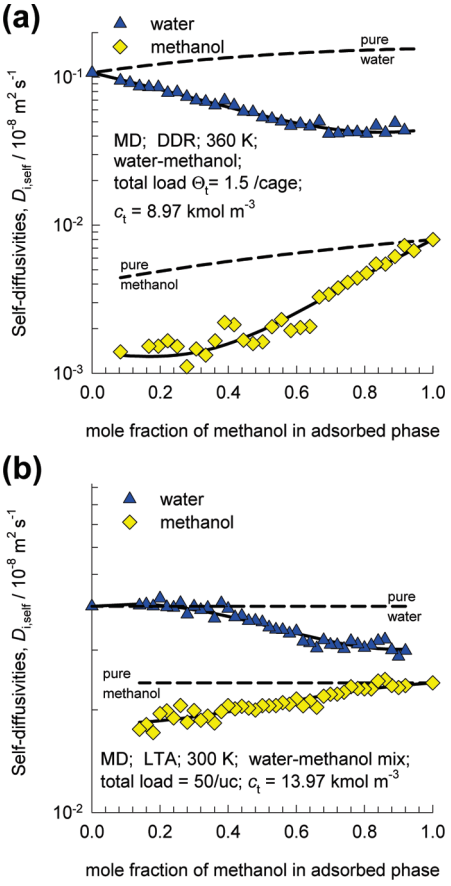

Figure 13. Self-diffusivities, $D_{i,self}$, in water−methanol mixtures of varying composition, and constant total mixture loading c_t. Key: (a) DDR at 360 K, and (b) LTA at 300 K. The dashed lines represent the $D_{i,self}$ of pure components, evaluated at the same occupancy θ_t as in the mixture.

Let us now consider water−alcohol diffusion in DDR, and LTA. For such structures, the commonly made assumption in practice is that the correlation effects are of negligible importance.[4,7] If this assumption is invoked, then eq 13 leads us to conclude that $D_{i,self} \approx Đ_i$. The MD data on $D_{i,self}$ for water−methanol mixtures in DDR are shown in Figure 13a. The dashed lines represent the $D_{i,self}$ of pure components, evaluated at the same occupancy θ_t as in the mixture. We note that the self-diffusivity of either component in lowered in the mixture, and this is ascribable to mutual hindering as discussed earlier for FAU. These data serve to rationalize the results of Kuhn et al.[7] who found that using the uncoupled M−S eqs 10, with pure component $Đ_i$ data, severely overpredicts the fluxes of both species in DDR permeation by about an order of magnitude. An analogous explanation holds for the water−ethanol permeation experiments.[6]

The self-diffusivity data for water−methanol mixtures in LTA (cf. in Figure 13b) also shows a significant reduction in the water diffusivity due to the presence of methanol. The corresponding reduction in methanol diffusivity is smaller, but not negligible. Pera-Titus et al.[4] found that matching their water−alcohol permeation experimental data for an LTA membrane using the uncoupled M−S eqs 10, requires values of $Đ_i$ that are significantly lower than the corresponding pure component values. Their observations can be rationalized by the mutual hindering effect highlighted in Figure 13b.

Water−alcohol diffusion in DDR and LTA is also distinctly different from diffusion of CO_2/CH_4 and CO_2/N_2 mixtures. In the latter cases CO_2 get preferentially lodged at the window regions,

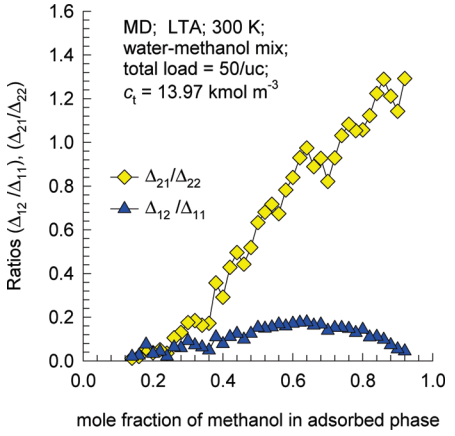

Figure 14. MD simulated values of Δ_{12}/Δ_{11}, and Δ_{21}/Δ_{22} for water−methanol mixtures of varying composition in LTA at 300 K. The total mixture loading is 50 molecules per unit cell, corresponding to c_t = 13.97 kmol m^{-3}.

hindering the transport of partner molecules.[16,24,25,79,96] The diffusivity of CO_2 in the mixture is unaffected by the partner species and there is no mutual hindering as for water−alcohol mixtures.

A further question remains unanswered. Is there any justification for use of uncoupled M−S eqs 10 for DDR and LTA, as assumed by Kuhn[6] and Pera-Titus,[4] or are the coupling effects of importance? The importance of coupling will be dictated by how large the ratios Δ_{12}/Δ_{11}, and Δ_{21}/Δ_{22} are with respect to unity. If the ratios are close to zero, then coupling effects can be neglected. MD data on water (1) and methanol (2) mixture diffusion in LTA are presented in Figure 14. At high methanol compositions, Δ_{21}/Δ_{22} tends to exceed unity, indicating that correlations become increasingly important for methanol transport. Put another way, we should expect methanol transport to be also influenced by the chemical potential driving force for water transport. Conversely the ratio Δ_{12}/Δ_{11} remains below about 0.1 for the entire compositions. This however does not imply that coupling effects can be neglected for water transport, because the chemical potential gradient driving force for methanol will be significantly higher than that of water, $\nabla\mu_2 \gg \nabla\mu_1$, causing $\Delta_{12}\nabla\mu_2$ to offer a non-negligible contribution to the fluxes calculated using eq 4. A similar conclusion can be expected to hold for water−alcohols diffusion in DDR; however the Δ_{ij} for mixture diffusion in DDR could not be determined with sufficient accuracy with MD.

5. Conclusions

Adsorption and diffusion of water−alcohol mixtures in FAU, MFI, LTA, and DDR have many characteristics that are distinctly different from those for nonpolar mixtures. Specifically, our studies lead to the following main observations and conclusions.

(1) For adsorption of pure water and alcohols, molecular clustering, induced by hydrogen bonding, causes the inverse thermodynamic factor $1/\Gamma_i$ to exceed unity for a range of concentrations c_i.

(2) For unary diffusion, when the extent of clustering is severe, and $1/\Gamma_i \gg 1$, the Fick diffusivity, D_i, can be lower than the self-diffusivity, $D_{i,self}$, for a range of concentrations. Also the T-dependence of the diffusivities may exhibit non-Arrhenius behavior.

(3) For water−alcohol mixtures, the hydrogen bonding between water and alcohol molecules is much more predominant that for water−water and alcohol−alcohol. As a consequence of this, the adsorption of binary water−methanol and water−ethanol mixtures show strong deviations from the predictions of the ideal adsorbed solution theory (IAST).

(4) The water−alcohol bonding also leaves its imprint on the mixture diffusion characteristics. The Maxwell−Stefan diffusivity, $Đ_i$, of either component in water−alcohol mixtures is lower than the corresponding values of the pure components. Furthermore, the binary exchange coefficient $Đ_{12}$ for water−alcohol mixtures is also significantly lower than either self-exchange coefficients $Đ_{11}$ and $Đ_{22}$ of the constituent species. This implies that correlation effects are significantly stronger in water−alcohol mixtures than for the constituent species. Both of the commonly used tenets of the M−S equations are invalidated for water−alcohols mixture diffusion.

(5) For zeolites such as LTA, DDR the use of the uncoupled M−S eqs 10 for water−alcohol permeation is not justified. Correlation effects do appear to play a role for mixtures, even though such effects are not present for pure components.

The inescapable conclusion to be drawn from the results of our investigations is that the estimation of the adsorption and diffusion behavior of water−alcohol mixtures using only pure component data on isotherms and diffusivities is not possible. Further work is necessary for development of reliable estimations, and our current work has this objective in focus.

Acknowledgment. R.K. acknowledges the grant of a TOP subsidy from The Netherlands Foundation for Fundamental Research (NWO−CW) for intensification of reactors. R.K. acknowledges helpful suggestions from Dr. D. Dubbeldam.

Notation

b_i	dual-Langmuir−Sips constant for species i, Pa$^{-v_i}$
c_i	concentration of species i, mol m^{-3}
$c_{i,sat}$	saturation capacity of species i, mol m^{-3}
c_t	total concentration in mixture, mol m^{-3}
D_i	Fick diffusivity of species i, m^2 s^{-1}
$D_{i,self}$	self-diffusivity of species i, m^2 s^{-1}
$Đ_{ii}$	self-exchange coefficient, m^2 s^{-1}
$Đ_i$	M−S diffusivity, m^2 s^{-1}
$Đ_{ij}$	M−S exchange coefficient defined by eq 1, m^2 s^{-1}
f_i	fluid phase fugacity of species i, Pa
n_i	number of molecules of species i in simulation box, dimensionless
N_i	molar flux of species i, based on crystalline framework cross-sectional area, mol m^{-2} s^{-1}
$\mathbf{r}_{l,i}(t)$	position vector for molecule l of species i at any time t, m
R	gas constant, 8.314 J mol^{-1} K^{-1}
t	time, s
T	absolute temperature, K
x_i	mole fraction of species i based on loading within pore, dimensionless

Glossary

Greek Letters

Δ_{ij}	Diffusivities defined by eq 4, m^2 s^{-1}
ϕ	fractional pore volume of zeolite, dimensionless

(96) Krishna, R.; van Baten, J. M. *Microporous Mesoporous Mater.* **2009**, *125*, 126–134.

Γ_i thermodynamic factor, dimensionless
μ_i molar chemical potential, J mol^{-1}
ν_i exponent in the dual-Langmuir−Sips isotherm, dimensionless
θ_i fractional occupancy of species i, dimensionless
Θ_i loading of i, molecules per cage

Subscripts

A, B referring to adsorption sites A and B
i referring to component i
sat referring to saturation conditions
t referring to total mixture

Vector and Matrix Notation

∇ gradient operator

Supporting Information Available: Text, tables, and figures providing details of the CBMC and MD simulation methodologies, details of the microporous structures (unit cell dimensions, accessible pore volume), pore landscapes, description of the force fields used, simulation data on isotherms, and diffusivities and movies (avi) showing animations of MD simulations for diffusion of water, methanol, ethanol, water−methanol, and water−ethanol in DDR, LTA, and ZIF-8 (these animations provide some qualitative indication of clustering). This material is available free of charge via the Internet at http://pubs.acs.org.